

The GRB luminosity function in the internal shock model confronted to observations

H. Zitouni^{1,2*}, F. Daigne^{1,3}, R. Mochkovich¹, and T. H. Zerguini²

¹ *Institut d’Astrophysique de Paris, UMR7095 CNRS, Université Pierre & Marie Curie-Paris 6, 98 bis boulevard Arago, 75014 Paris, France.*

² *Université des Sciences et Technologies Houari Boumedienne, BP 32 16123 Bab-Ezzouar Alger, Algeria.*

³ *Institut Universitaire de France.*

Accepted 2008 February 21. Received 2008 January 15; in original form 2007 October 26

ABSTRACT

We compute the expected luminosity function of GRBs in the context of the internal shock model. We assume that GRB central engines generate relativistic outflows characterized by the respective distributions of injected kinetic power \dot{E} and contrast in Lorentz factor $\kappa = \Gamma_{\max}/\Gamma_{\min}$. We find that if the distribution of contrast extends down to values close to unity (i.e. if both highly variable and smooth outflows can exist) the luminosity function has two branches. At high luminosity it follows the distribution of \dot{E} while at low luminosity it is close to a power law of slope -0.5 . We then examine if existing data can constrain the luminosity function. Using the $\log N - \log P$ curve, the E_p distribution of bright BATSE bursts and the XRF/GRB ratio obtained by HETE2 we show that single and broken power-laws can provide equally good fits of these data. Present observations are therefore unable to favor one form of the other. However when a broken power-law is adopted they clearly indicate a low luminosity slope $\simeq -0.6 \pm 0.2$, compatible with the prediction of the internal shock model.

Key words: gamma-rays: bursts; stars: luminosity function; methods: statistical

1 INTRODUCTION

The isotropic luminosity of long gamma-ray bursts is known to cover a wide range from underluminous, nearby bursts such as GRB 980425 or GRB 060218 (with $L \lesssim 10^{47}$ erg.s⁻¹) to ultrabright objects like GRB 990123 ($L \gtrsim 10^{53}$ erg.s⁻¹). While it has been suggested that the weakest GRBs could simply be normal events seen off-axis (Yamazaki et al. 2003), this possibility has been recently discarded both from limits on afterglow brightness and for statistical reasons (Soderberg et al. 2004; Daigne & Mochkovitch 2007). The difference of six orders of magnitude between the brightest and weakest GRBs is therefore probably real. The parameters (stellar rotation, metallicity, etc.) which are responsible for this diversity in radiated power are not known. However, in the restricted range $10^{51} \lesssim L \lesssim 10^{53}$ erg.s⁻¹ the value of the isotropic luminosity is possibly fixed by the opening angle of the jet which may always carry the same characteristic energy (Frail et al. 2001).

The purpose of this paper is to see how basic theoretical ideas and existing data can be used to constrain the GRB luminosity function (hereafter LF) $p(L)$. First, we should insist that $p(L)$ here represents the “apparent” LF which includes

viewing angle effects and beaming statistics (i.e. bursts with narrow jets are more likely seen off-axis and therefore under-represented in the distribution). It is therefore different from the “intrinsic” LF $p_0(L)$ which would be obtained with all GRBs seen on-axis. In the lack of a complete, volume limited sample of GRBs with known redshift, only indirect observational indicators such as the $\log N - \log P$ plot can constrain the LF. These indicators however depend not only on $p(L)$ but also on the GRB rate and spectral energy distribution. The simplest possible form for $p(L)$ is a single power law $p(L) \propto L^{-\delta}$ between L_{\min} and L_{\max} . Together with the parameters describing the GRB rate and spectral shape, δ , L_{\min} and L_{\max} can be adjusted to provide the best possible fit of the available indicators. Considering the mixing of the LF with other quantities in the fitting process it is remarkable that studies using different observational constraints have converged to a similar value of the slope $\delta \sim 1.5 - 1.7$ (e.g. Firmani et al. 2004; Daigne & Mochkovitch 2007).

In a second step one can consider the more general case of a broken power law LF with now five parameters: L_{\min} , L_{\max} , the two slopes δ_1 and δ_2 and the break luminosity L_b . We will see in Sect.2 that there is some indication that the internal shock model of GRBs can produce a broken power law LF and we want to check if it is also favored by the existing observational data. As in our previous study we have used a Monte Carlo method to generate a large number

* E-mail: zitouni@iap.fr (HZ); daigne@iap.fr (FD); mochkovich@iap.fr (RM)

of synthetic events where the parameters defining the burst properties are varied within fixed intervals. Preferred values of the parameters are those which yield the minimum χ^2 for a given set of observational constraints. We summarize these constraints and present the Monte Carlo simulations in Sect.3. We discuss our results in Sect.4 and Sect.5 is our conclusion.

2 THE GRB LUMINOSITY FUNCTION IN THE INTERNAL SHOCK MODEL

The internal shock model (Rees & Meszaros 1994) is the most discussed solution to explain the prompt gamma-ray emission in GRBs. In this section, we demonstrate that it naturally leads to a broken power-law LF with a low-luminosity slope close to -0.5 .

2.1 Internal shock efficiency and luminosity function

In the context of the internal shock model (Rees & Meszaros 1994), the prompt gamma-ray emission is produced by relativistic electrons accelerated in internal shocks propagating within a relativistic outflow. The (isotropic equivalent) radiated luminosity L is then a fraction of the (isotropic equivalent) rate of kinetic energy injected in the flow \dot{E}

$$L = f(\kappa) \dot{E} . \quad (1)$$

The efficiency $f(\kappa)$ is the product of three terms

$$f(\kappa) \simeq f_{\text{rad}} \epsilon_e f_{\text{dyn}}(\kappa) , \quad (2)$$

where (i) $f_{\text{dyn}}(\kappa)$ is the fraction of the kinetic energy which is converted by internal shocks into internal energy (“dynamical efficiency”). This fraction depends mainly on the contrast $\kappa = \Gamma_{\text{max}}/\Gamma_{\text{min}}$ of the Lorentz factor distribution in the relativistic outflow; (ii) ϵ_e is the fraction of this dissipated energy which is injected into relativistic electrons. We assume that ϵ_e is close to the equipartition value $\epsilon_e = 1/3$, as it is a necessary condition to have an efficient mechanism; (iii) f_{rad} is the fraction of the electron energy which is radiated. To explain the observed variability timescales in GRB lightcurves and to maintain a reasonable efficiency, the relativistic electrons must be in the fast cooling regime, which means that their radiative timescale is very short compared to the hydrodynamical timescales in the outflow. In this case, we have $f_{\text{rad}} \simeq 1$.

The GRB LF in the internal shock model is therefore related to the physics of the relativistic ejection by the central engine. We assume that the contrast κ is distributed between κ_{min} and κ_{max} with a density of probability $\psi(\kappa)$ and that \dot{E} is distributed between \dot{E}_{min} and \dot{E}_{max} with a density of probability $\phi(\dot{E})$. The minimum and maximum radiated luminosities are therefore

$$L_{\text{min}} = f(\kappa_{\text{min}}) \dot{E}_{\text{min}} \quad (3)$$

and

$$L_{\text{max}} = f(\kappa_{\text{max}}) \dot{E}_{\text{max}} . \quad (4)$$

For $L_{\text{min}} \leq L \leq L_{\text{max}}$, the probability to have a radiated luminosity in the interval $[L; L + dL]$ is $p_0(L)dL$, where the intrinsic LF $p_0(L)$ is given by

$$p_0(L) = \int_{\text{max}}^{\text{max}} \left(\kappa_{\text{max}}; f^{-1}\left(\frac{L}{\dot{E}_{\text{min}}}\right) \right) \frac{\psi(\kappa)}{f(\kappa)} \phi\left(\frac{L}{f(\kappa)}\right) d\kappa . \quad (5)$$

2.2 The case of a power-law distribution of kinetic energy flux

We assume that the injection rate of kinetic energy in the relativistic outflow follows a power-law distribution

$$\phi(\dot{E}) \simeq \frac{\delta - 1}{\dot{E}_{\text{min}}} \left(\frac{\dot{E}}{\dot{E}_{\text{min}}} \right)^{\delta} , \quad (6)$$

with $\dot{E}_{\text{max}} \gg \dot{E}_{\text{min}}$. Then, the GRB LF given by equation (5) becomes

$$p_0(L) \simeq \frac{\delta - 1}{L_*} \left(\frac{L}{L_*} \right)^{-\delta} \times \int_{\text{max}}^{\text{min}} \left(\kappa_{\text{max}}; f^{-1}\left(\frac{L}{\dot{E}_{\text{min}}}\right) \right) \psi(\kappa) \left(\frac{f(\kappa)}{f(\kappa_{\text{max}})} \right)^{\delta-1} d\kappa , \quad (7)$$

where the luminosity L_* is defined by

$$L_* = f(\kappa_{\text{max}}) \dot{E}_{\text{min}} . \quad (8)$$

Let us now consider a first case where GRB central engines can produce all kinds of outflows, from highly variable to perfectly smooth. In this case, the minimum contrast is $\kappa_{\text{min}} = 1$, corresponding to a minimum efficiency $f(\kappa_{\text{min}}) = 0$, as no internal shocks can develop in an outflow with a constant Lorentz factor. The first limit in the integral in equation (7) is then always given by $f^{-1}(L/\dot{E}_{\text{max}})$ and the LF is made of two branches :

• **High-luminosity branch.** For $L_* \leq L \leq L_{\text{max}}$, the second limit in the integral is κ_{max} , which leads to

$$p_0(L) \simeq \frac{\delta - 1}{L_*} \left(\frac{L}{L_*} \right)^{-\delta} f(\kappa_{\text{max}}) \times \int_{L/L_{\text{max}}}^1 dx x^{\delta-1} \frac{\psi\left(f^{-1}(xf(\kappa_{\text{max}}))\right)}{f'\left(f^{-1}(xf(\kappa_{\text{max}}))\right)} . \quad (9)$$

For $L_* \leq L \ll L_{\text{max}}$, $L/L_{\text{max}} \rightarrow 0$ so that the integral is nearly constant. The high-luminosity branch of the LF is therefore very close to a power-law of slope $-\delta$, i.e. the slope of the intrinsic distribution of injected kinetic power.

• **Low-luminosity branch.** For $L_{\text{min}} = 0 \leq L \leq L_*$, the second limit in the integral is $f^{-1}(L/\dot{E}_{\text{min}})$, which leads to

$$p_0(L) \simeq \frac{\delta - 1}{L_*} \left(\frac{L}{L_*} \right)^{-\delta} f(\kappa_{\text{max}}) \times \int_{L/L_{\text{max}}}^{L/L_*} dx x^{\delta-1} \frac{\psi\left(f^{-1}(xf(\kappa_{\text{max}}))\right)}{f'\left(f^{-1}(xf(\kappa_{\text{max}}))\right)} . \quad (10)$$

The LF is determined by the behaviour of the efficiency $f(\kappa)$ at very low contrast. We assume that $f(\kappa) \simeq f_0(\kappa - 1)^\alpha$ for $\kappa \rightarrow 1$ and we define $L_0 = f_0 \dot{E}_{\min}$. Then, for $L \ll L_*$, we have

$$p_0(L) \simeq \frac{\delta - 1}{L_0} \left(\frac{L}{L_0} \right)^{\frac{1}{\alpha} - 1} \frac{\psi(1)}{1 + \alpha(\delta - 1)}. \quad (11)$$

We therefore find that for $L \ll L_*$ and $\kappa_{\min} = 1$, the LF is also a power-law, with however a slope $1/\alpha - 1$ which does not depend on the slope of the intrinsic distribution of injected kinetic power.

Then, the predicted intrinsic GRB LF in the internal shock model is a broken power-law, of slope $1/\alpha - 1$ at low-luminosity and $-\delta$ at high luminosity, with a break luminosity $L_* = f(\kappa_{\max}) \dot{E}_{\min}$. The shape of $p_0(L)$ at the transition ($L \sim L_*$) is related to the distribution of the contrast $\psi(\kappa)$. If $\kappa_{\min} \neq 1$ this result remains valid as long as very low contrasts can be achieved ($\kappa_{\min} \lesssim 1.1$; see figure 1, left panel). Note that the analysis of the internal shock model parameter space made by Barraud et al. (2005) shows that very low contrasts are necessary to produce soft GRBs such as X-ray rich GRBs (XRRs) and X-ray flashes (XRFs). However, if it happens that GRB central engines never produce smooth outflows (i.e. if κ_{\min} is not close to unity), the calculation made above remains valid for the high-luminosity branch, which is still a power-law of slope $-\delta$, but the low-luminosity branch is much reduced and no more a power-law.

Finally, we have briefly considered the case where the distribution of injected kinetic power $\phi(\dot{E})$ is not a power-law. For example, for a log-normal distribution peaking at \dot{E}_* , we again obtain that the intrinsic LF follows $\phi(\dot{E})$ at high luminosity and is a power-law of slope -0.5 at low-luminosity, with a transition at $L_* \sim f(\kappa_{\max}) \dot{E}_*$.

2.3 A simple model for the internal shock efficiency

To investigate more precisely the GRB LF, we need to know the form of the efficiency $f(\kappa)$. As shown in Daigne & Mochkovitch (1998), it is a priori a complex function of the initial distribution of the Lorentz factor and the kinetic energy in the relativistic outflow. However, one can make a simple estimate by using the toy model developed in Daigne & Mochkovitch (2003); Barraud et al. (2005) where we only consider direct collisions between two equal-mass relativistic shells. In this case, the efficiency is simply given by

$$f(\kappa) \simeq \epsilon_e \times \frac{(\sqrt{\kappa} - 1)^2}{\kappa + 1}. \quad (12)$$

For low contrast, it behaves as $f(\kappa) \simeq \epsilon_e(\kappa - 1)^2/8$, which corresponds to $f_0 = \epsilon_e/8$ and $\alpha = 2$. In addition to this toy model which gives an explicit expression for the efficiency we have used our detailed internal shock code (Daigne & Mochkovitch 1998) and checked the quadratic dependence of $f(\kappa)$ in $(\kappa - 1)$. Also notice that the result $\alpha = 2$ will remain valid even if ϵ_e is not strictly constant, as long as it does not vary as some power of $(\kappa - 1)$ at low κ

($\epsilon_e \propto (\kappa - 1)$ leading for example to $\alpha = 3$ and $p_0(L) \propto L^{-2/3}$ at low luminosity).

Assuming a constant ϵ_e , we have plotted the resulting GRB LF in figure 1. The intrinsic distribution of injected kinetic power is defined between $\dot{E}_{\min} = 10^{52} \text{ erg s}^{-1}$ and $\dot{E}_{\max} = 10^{54} \text{ erg s}^{-1}$ and has a slope $-\delta = -1.7$. We have fixed the maximum value of the contrast to $\kappa_{\max} = 10$, so that $L_* \simeq 1.4 \times 10^{51} \text{ erg s}^{-1}$. In the left panel, we have assumed that the logarithm of the contrast κ is uniformly distributed between $\log \kappa_{\min}$ and $\log \kappa_{\max}$, with $\kappa_{\min} = 1, 1.001, 1.01, 1.1$ or 2 . For all values of κ_{\min} , the high-luminosity branch is the same power-law of slope $-\delta = -1.7$. For $\kappa_{\min} = 1$, the low-luminosity branch extends down to $L = 0$ and is the expected power-law of slope $1/\alpha - 1 = -1/2$. This branch is still clearly visible for $\kappa_{\min} = 1.001, 1.01$ and 1.1 but nearly disappears for $\kappa_{\min} = 2$. For even higher values of κ_{\min} , only the high-luminosity power-law remains.

We have tested in the right panel of figure 1 that for other choices of the distribution of contrast $\psi(\kappa)$, the GRB LF is not affected (the two slopes remain unchanged) except for the shape of the transition at $L \sim L_*$. A low-luminosity branch of slope ~ -0.5 in the intrinsic LF is therefore a robust prediction of the internal shock model, as long as GRB central engines can produce smooth outflows (very low contrasts). The low-luminosity branch will however manifest itself only if $L_* = f(\kappa_{\max}) \dot{E}_{\min}$ is large enough; otherwise the observationally accessible part of the LF of cosmological GRBs will behave as a single power-law (in figure 1, $L_* \simeq 1.4 \times 10^{51} \text{ erg s}^{-1}$).

2.4 Apparent GRB luminosity function

The GRB LF that has been derived from the internal shock model is intrinsic. If GRB ejecta have a jet-like geometry with an opening angle $\Delta\theta$ which is not correlated to the kinetic energy flux \dot{E} , the apparent LF above L_* has the same shape as the intrinsic one since the fraction of observed GRBs does not depend on \dot{E} . At lower luminosities, two effects are in competition : low-luminosity bursts can be due to a low internal shock efficiency and/or a large viewing angle. Close to L_* , the first effect dominates and the slope is still very close to -0.5 as predicted above. At very low luminosity, the second effect takes over. It can be shown that the slope then becomes close to $-7/6$. Observing this final slope seems difficult as it involves the detection of very faint bursts. However viewing angle effects already modify the low-luminosity slope below the break where it progressively departs from its intrinsic value -0.5 (see Fig.2).

If it happens that the opening angle $\Delta\theta$ is correlated with \dot{E} , the apparent $p(L)$ will be also different from the intrinsic one at high luminosity. A possible correlation could be

$$\dot{E}(1 - \cos \Delta\theta) = \text{cst} = \dot{E}_{\min}. \quad (13)$$

meaning that the true kinetic energy rate is the same for all bursts. Such an assumption is motivated by the evidence that there might be a standard energy reservoir in GRBs (Frail et al. 2001). In this case, the high-luminosity branch (above L_*) of $p(L)$ has a slope $-(1 + \delta)$, where $-\delta$ is the slope of the intrinsic LF. This is illustrated in figure 2 (right panel).

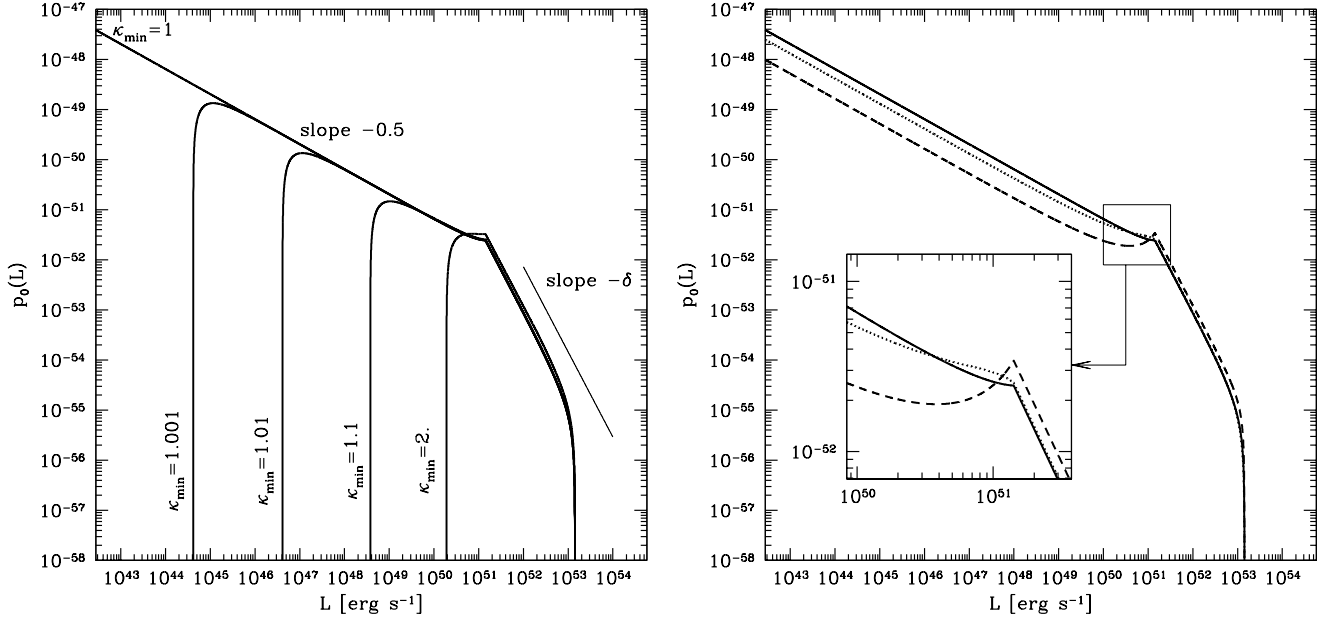


Figure 1. The intrinsic GRB LF in the internal shock model. The function $p_0(L)$ is plotted, assuming an intrinsic distribution of injected kinetic power \dot{E} that is a power-law of slope $-\delta = -1.7$ between $\dot{E}_{\min} = 10^{52}$ erg s $^{-1}$ and $\dot{E}_{\max} = 10^{54}$ erg s $^{-1}$. This function $\phi(\dot{E})$ is plotted as a thin line in the left panel. *Left:* effect of the minimum constraint κ_{\min} . We assume that $\log \kappa$ is uniformly distributed between $\log \kappa_{\min}$ and $\log \kappa_{\max}$ with $\kappa_{\min} = 1, 1.001, 1.01, 1.1$ and $\kappa_{\max} = 10$. *Right panel:* effect of the shape of the distribution of contrast. We fix $\kappa_{\min} = 1$ and $\kappa_{\max} = 10$ and consider three different shapes for the distribution of contrast $\psi(\kappa)$: (i) $\log \kappa$ uniformly distributed (solid line); (ii) $\psi(\kappa) \propto \exp(-\kappa/4)$ (dotted line); (iii) κ uniformly distributed (dashed line). An inset shows the transition at $L_* = 1.4 \times 10^{51}$ erg s $^{-1}$ in more details.

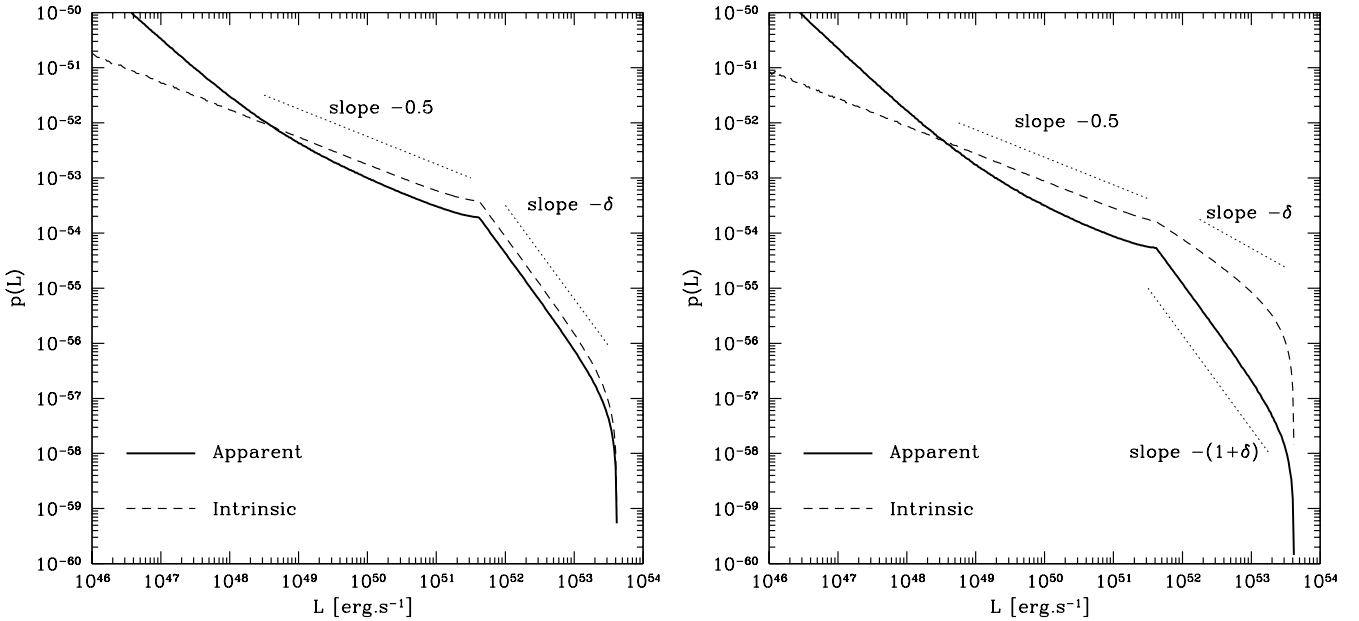


Figure 2. The apparent GRB LF in the internal shock model. The intrinsic LF $p_0(L)$ is plotted in dashed line for $\log(\kappa)$ uniformly distributed with $\kappa_{\min} = 1$ and $\kappa_{\max} = 10$, and for \dot{E} following a power-law distribution of slope $-\delta$ between $\dot{E}_{\min} = 10^{52}$ erg s $^{-1}$ and $\dot{E}_{\max} = 10^{54}$ erg s $^{-1}$. The corresponding apparent LF is plotted in solid line. *Left:* the opening angle is distributed between 0 and $\pi/2$ according to $p(\Delta\theta) = \sin \Delta\theta$ (uniformly distributed opening angle). We adopt $\delta = -1.7$. *Right:* the opening angle is correlated with the kinetic energy flux according to Eq. (13). We adopt $\delta = -0.7$.

3 CONSTRAINING THE GRB LUMINOSITY FUNCTION

3.1 Monte Carlo simulations

We use Monte Carlo simulations to constrain the GRB LF from observations. The method is described in details in Daigne et al. (2006). We recall here the main lines :

- **Properties of the long GRB population.** We characterize this population by the intrinsic distribution of several physical properties : (1) the comoving rate. We define $\mathcal{R}_{\text{GRB}}(z)$ ($\text{Mpc}^{-3} \text{ yr}^{-1}$) as the GRB comoving rate at redshift z . We assume that the GRB comoving rate is proportional to the star formation rate (SFR). Following Porciani & Madau (2001), this can be written as $\mathcal{R}_{\text{GRB}} = k \times \mathcal{R}_{\text{SN}}$, where \mathcal{R}_{SN} is the comoving rate of collapses of massive stars above $8 M_{\odot}$. We consider three possible scenarios (see Fig.1 in Daigne et al. (2006) and reference therein), that all fit the observed SFR up to $z \sim 2 - 3$: SFR_1 where the SFR decreases for $z \gtrsim 2$, SFR_2 where it is constant for $z \gtrsim 2$ and SFR_3 where it increases for $z \gtrsim 2$. In this last case, we have to assume a maximum redshift for star formation. We adopt $z_{\text{max}} = 20$; (2) the LF. In this paper, for simplicity, we do not discuss evolutionary effects. Therefore, the probability density $p(L)$ of the isotropic equivalent luminosity L does not depend on z . In Daigne et al. (2006) we only considered the case of a power-law distribution, with $p(L) \propto L^{-\delta}$ for $L_{\text{min}} \leq L \leq L_{\text{max}}$. Here, we test more complicated LFs, i.e. broken power-laws defined by

$$p(L) \propto \begin{cases} L^{-\delta_1} & \text{for } L_{\text{min}} \leq L \leq L_b, \\ L^{-\delta_2} & \text{for } L_b \leq L \leq L_{\text{max}}; \end{cases} \quad (14)$$

- (3) the distributions of intrinsic spectral parameters. We assume that the GRB photon spectrum is given by a broken power-law with a break at energy E_p (Band et al. 1993) and a slope $-\alpha$ (resp. $-\beta$) at low (resp. high) energy. We checked that the use of the more realistic spectrum shape proposed by Band et al. (1993) does not affect our conclusions. The slopes α and β are given the distributions observed in a sample of BATSE bright long GRBs (Preece et al. 2000). For the peak energy E_p we consider two possible cases, either a log-normal distribution, with a mean value $E_{p,0}$ and a dispersion $\sigma = 0.3$ dex (hereafter “log-normal E_p distribution”) or an intrinsic correlation between the spectral properties and the luminosity (hereafter “Amati-like relation”), as found by Amati et al. (2002); Amati (2006). We assume in this case that

$$E_p = 380 \text{ keV} \left(\frac{L}{1.6 \times 10^{52} \text{ erg s}^{-1}} \right)^{0.43}, \quad (15)$$

with a normal dispersion $\sigma = 0.2$ dex in agreement with observations (Yonetoku et al. (2004); Ghirlanda et al. (2005), see however Nakar & Piran (2005); Band & Preece (2005) who tested this relation against BATSE data and concluded that selection effects were dominant).

- **Criteria of detection by several instruments.** With the assumptions listed above, a GRB in the simulation is characterized by a redshift z , a peak luminosity L , and a spectrum defined by E_p , α and β . It is therefore possible to compute the observed peak flux in any spectral band. Using the known sensitivity of several instruments (see Daigne et al. (2006) for the detailed thresholds we use), we

can determine if a given burst is detected by the following experiments : (i) BATSE, for which we define two samples in our synthetic bursts (all BATSE bursts and bright BATSE bursts) ; (ii) HETE2, for which we test the detection either by the gamma-ray (FREGATE) or the X-ray (WXM) instrument; and (iii) SWIFT, for which we test the detection by the gamma-ray instrument only (BAT) and we also define two samples (all SWIFT bursts and bright SWIFT bursts). It is then possible to compute simulated observed distribution of various quantities to compare them with real data.

- **Observational constrains.** We use three different kind of observations: (1) the $\log N - \log P$ diagram of BATSE bursts (Stern et al. 2000, 2001); (2) the observed peak energy distribution of long bright GRBs (Preece et al. 2000); and (3) the observed fraction of soft GRBs (X-ray Flashes and X-ray rich GRBs) in the sample of GRBs detected by HETE2 (Sakamoto et al. 2005). The $\log N - \log P$ diagram is broadly used for such kind of studies but we have shown in Daigne et al. (2006) that (2) and (3) are good complements to better constrain the parameters of the GRB population.

Depending on the assumptions on the spectral properties, we have 4 or 5 free parameters for a single power-law LF (k , L_{min} , L_{max} , δ and $E_{p,0}$ in the case of a log-normal distribution). The observational constraints correspond to 41 data points (see figure 4 : 30 data points in the $\log N - \log P$ diagram published by Stern et al. (2001); 10 points for the E_p distribution published by Preece et al. (2000) which has been rebinned in 10 logarithmic bins of size 0.2 dex between 15.8 keV and 1.58 MeV; 1 point for the fraction of soft GRBs). We have therefore 37 or 36 degrees of freedom. The numerical procedure is the following : for a set of parameters, we generate randomly a population of 10^5 GRBs using the distribution defined above, we then compute the simulated distributions of observed peak flux, peak energy, etc. and we compare them to real data, by computing a χ^2 . We do that for a large number of sets of parameters, randomly chosen to explore a large space. We always find a clear minimum χ_{min}^2 of χ^2 and we define as “best models” all models with $\chi_{\text{min}}^2 \leq \chi^2 \leq \chi_{\text{min}}^2 + \Delta\chi^2$, where $\Delta\chi^2$ defines the 1σ level and is computed from the number of degrees of freedom.

The main results obtained in Daigne et al. (2006) are (1) that SFR_3 is strongly favored by the observed redshift distribution of SWIFT bursts. But a SFR rising at large z appears unlikely as it would overproduce metals at early times. This is therefore an indirect indication in favor of a GRB rate that does not directly follow the SFR, for instance due to an evolution with redshift of the efficiency of massive stars to produce GRBs¹; (2) with this SFR_3 , both the “Amati-like relation” and the “log-normal E_p distribution” give good fits to the observational constraints

¹ In Daigne et al. (2006), we have tested whether an evolution of the LF could reconcile the SFR_1 or SFR_2 scenario with Swift data. We found that this is very unlikely as the evolution should be strong ($L \propto (1+z)^\nu$ with $\nu > 2$). We therefore conclude that the evolution of the GRB rate (i.e the evolution of the stellar efficiency to produce GRBs) is dominant compared to a possible evolution of the LF.

listed above. Best model parameters of the LF do not vary too much from one scenario to another : the slope is well determined, $\delta \sim 1.5 - 1.7$, but the minimum and maximum luminosities are not so well constrained, with $L_{\min} \sim 0.8 - 3 \times 10^{50} \text{ erg s}^{-1}$ and $L_{\max} \sim 3 - 5 \times 10^{53} \text{ erg s}^{-1}$. It is interesting to note that with a different methodology, several groups have confirmed our conclusions on the GRB comoving rate (Le & Dermer 2007; Guetta & Piran 2007; Kistler et al. 2007).

In this paper, we present the results of additional simulations that we have carried out to test if the GRB LF can be a broken power-law. With two supplementary parameters (the break luminosity L_b and the second slope), we have now 6 (resp. 7) free parameters in the Amati-like relation case (resp. the case of a log-normal peak energy distribution). It is difficult to constrain accurately so many parameters with Monte Carlo simulations. Therefore, we have chosen to keep the maximum luminosity constant in all our simulations. We adopt $L_{\max} = 10^{53.5} \text{ erg s}^{-1}$, according to our previous study (Daigne et al. 2006). We also keep L_{\min} constant, and equal to a low value corresponding to weak GRBs that cannot be detected at cosmological distance. We usually adopt $L_{\min} = 10^{45} \text{ erg s}^{-1}$ but we have also tested other values (see next section). Keeping these two luminosities constant in our Monte Carlo simulation, we have the same number of degrees of freedom than in the model with a simple power-law LF.

3.2 Results

In our whole new set of simulations, we always find a clear minimum of χ^2 . The parameters of the best model, as well as 1 σ error bars are listed in table 1. As can be seen, we focus on the scenario where the comoving GRB rate follows SFR_3 and the peak energy is given by the Amati-like relation. For comparison, we also give the parameters of two reference models with a single power-law LF (Daigne et al. 2006). Figure 3 illustrates, in the case $\text{SFR}_3 + \text{Amati-like}$ relation, the position of the best models in the parameter space of the LF. As can be seen, the low-luminosity slope is strongly constrained to be small, $\delta_1 \lesssim 1$, with a mean value $\delta_1 \sim 0.6$, while the high-luminosity slope is larger, $\delta_2 \gtrsim 1.4$, with a mean value $\delta_2 \sim 1.7$. The break luminosity (right panel) is not so well constrained with best models having $L_b \simeq 4 \times 10^{50} - 6 \times 10^{51} \text{ erg s}^{-1}$. Figure 4 compares the fit of the data points ($\log N - \log P$ diagram and E_p distribution) with the best model obtained either with a power-law or a broken power-law LF. Both models are in good agreement with data, without a preference for one or the other. This is also indicated by the value of the reduced minimum χ^2 in both cases : 1.4 (power-law) and 1.3 (broken power-law) for 37 degrees of freedom.

Figure 5 shows – for the best model – the LF as well as the luminosity distribution of bursts detected by BATSE, HETE2 and SWIFT. It appears that the high-luminosity branch above L_b is extremely close to the best model single power-law LF (thin line). Below a few $10^{49} \text{ erg s}^{-1}$ (corresponding to the lowest values of the constraint, $\kappa \lesssim 1.2$), the fraction of detected GRBs is extremely low (less than 10^{-4} of the total). The two models (power-law vs broken power-law) differ in the $10^{49} - 10^{51} \text{ erg s}^{-1}$ range, where

the fraction of detected bursts is still small (less than 20% of the total) with therefore little effect on the observable quantities.

These results indicate that present data are not sufficient to distinguish between a power-law and a broken power-law LF. Both models can provide equally good fits to the observations. It is however interesting that a broken power-law remains allowed, as there are good theoretical arguments in favor of such a shape (see Sect.2). Table 1 show that the properties of the broken power-law LF remain very stable as long as L_{\min} is kept to a low value ($L_{\min} \lesssim 10^{48} \text{ erg s}^{-1}$): the position of the break and especially the values of the two slopes are not changing much, even for different GRB rates (SFR_1 and SFR_2 have also been tested). It seems however that the broken power-law LF is more sensitive to the assumptions on the spectral parameters. In the case where the spectral properties are not correlated to the luminosity (log-normal peak energy distribution), the low-luminosity slope is not too different from the “Amati-like relation” case ($\delta_1 \simeq 0.7$ instead of 0.6), but the break luminosity is larger ($L_b \simeq 10^{51-52}$ instead of $10^{50-51} \text{ erg s}^{-1}$) and the high-luminosity branch is steeper ($\delta_2 \simeq 1.8 - 2.4$ instead of 1.7).

These results can be partially compared to other studies. Based on an analysis of the BATSE $\log N - \log P$ diagram, Stern et al. (2002) have tested several shapes of GRB LFs, including a power-law and a broken power-law. Their assumptions concerning GRB spectra are different from those chosen in the present paper but are very close to our “log-normal peak energy distribution” scenario. For a GRB rate similar to our SFR_3 , they find $\delta_1 \simeq 1.3 - 1.6$, $\delta_2 \gtrsim 3$ and $L_b \simeq 10^{51} - 6 \times 10^{52} \text{ erg s}^{-1}$. Whereas we are in reasonable agreement for the high luminosity slope, there is a large discrepancy for the low-luminosity branch, which is much steeper in their study. To understand the origin of this discrepancy, we made an additional simulation where we force $\delta_1 = 1.3$ and let δ_2 and L_b free. We find that a good fit to the $\log N - \log P$ diagram can be found but that the peak energy distribution is not reproduced, which stresses the importance of this additional constrain in our study. Firmani et al. (2004) have presented a set of Monte Carlo simulations with assumptions on the intrinsic GRB properties that are very similar to ours but different observational constraints, as they fit the distribution of BATSE pseudo-redshifts obtained from the luminosity–variability correlation (Fenimore & Ramirez-Ruiz 2000). For the case with an intrinsic correlation between the luminosity and the spectral properties (Amati-like case) they find a break at $L_b \simeq 3 \times 10^{52} \text{ erg s}^{-1}$ with the low and high-luminosity slopes equal to $\delta_1 \simeq 0.8$ and $\delta_2 \simeq 2.1$. Taking into account the differences in the two approaches, the agreement between this study and our result is satisfactory, especially for the slopes. More recently, Guetta et al. (2005); Guetta & Piran (2007) have also studied the GRB rate and LF using the recent results from SWIFT. Their analysis is based on the use of the $\log N - \log P$ diagram only and they assume a very simplified GRB spectral shape, that is a power-law spectrum of photon index -1.6 . For SFR_3 , they find a break luminosity $L_b \simeq 4 \times 10^{51} \text{ erg.s}^{-1}$ and low and high luminosity slopes $\delta_1 \simeq 0.1$ and $\delta_2 \simeq 2$, with large error

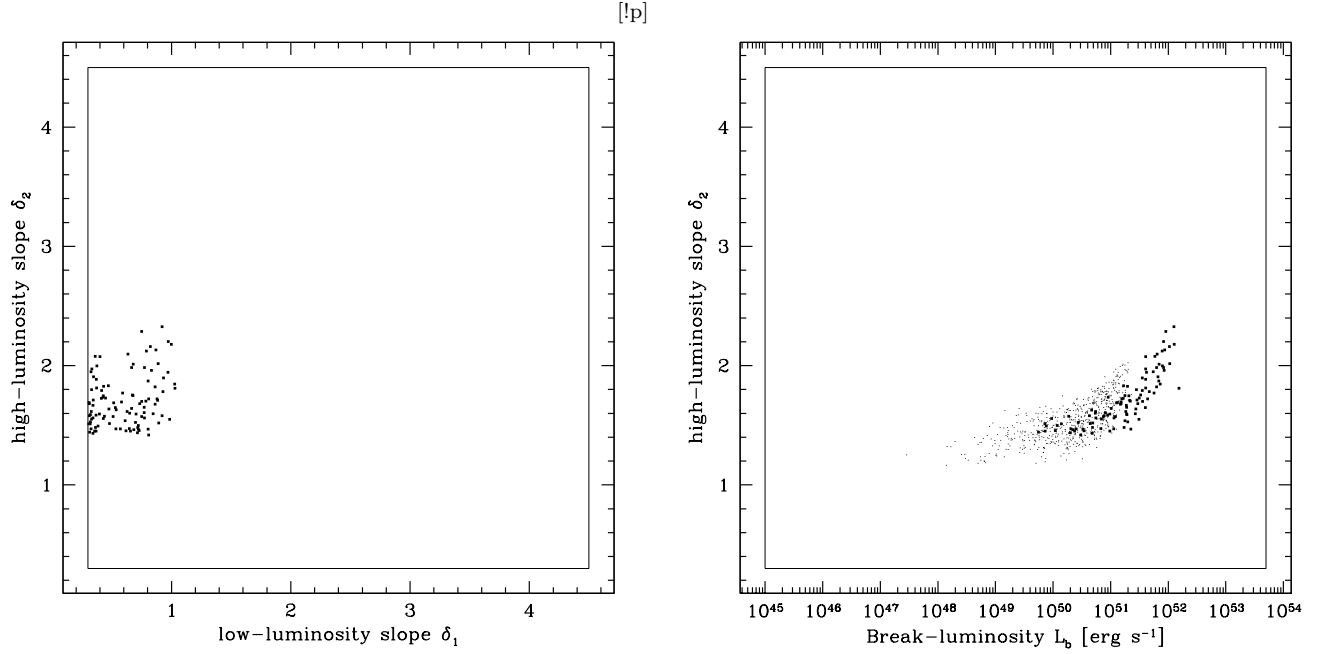


Figure 3. Parameter space (SFR₃, Amati-like relation) : we plot the location of the best models (1σ level) for a broken power-law LF with fixed minimum and maximum luminosities $L_{\min} = 10^{45}$ erg s⁻¹ and $L_{\max} = 10^{53.5}$ erg s⁻¹ (big dots). The range of parameters explored in the Monte Carlo is indicated with a box. In the right panel, the best models for a single power-law LF (Daigne et al. 2006) are also plotted with small dots (in this case the x-axis stands for the minimum luminosity and the y-axis for the slope).

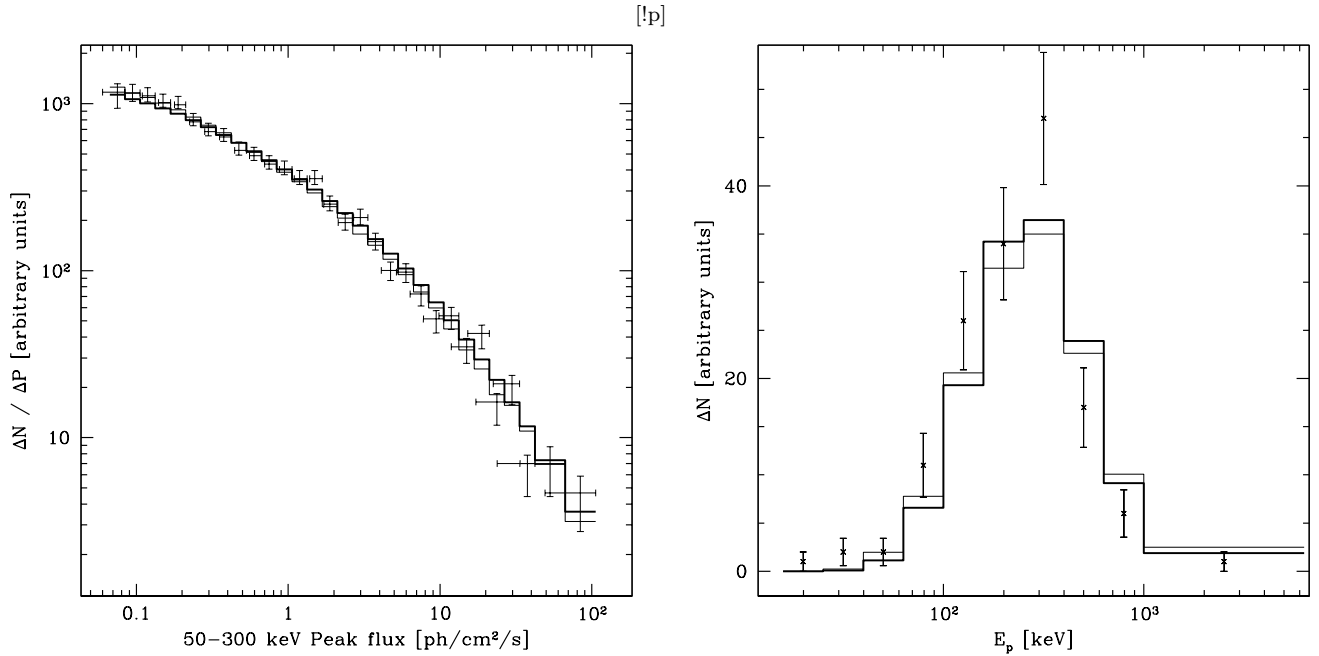


Figure 4. Best model (SFR₃, Amati-like relation). *Left:* the simulated $\log N - \log P$ diagram of BATSE is plotted as well as BATSE data (Stern et al. 2002); *right:* the simulated peak energy distribution of bright BATSE bursts is plotted as well as the observed distribution (Preece et al. 2000). In both panels, the best model for a broken power-law LF with fixed minimum and maximum luminosities $L_{\min} = 10^{45}$ erg s⁻¹ and $L_{\max} = 10^{53.5}$ erg s⁻¹ is plotted in thick line. For comparison the best model for a single power-law LF obtained in Daigne et al. (2006) is plotted in thin line.

Table 1. Best models: parameters.

SFR	$\log L_{\min}$ (erg s ⁻¹)	$\log L_b$ (erg s ⁻¹)	$\log L_{\max}$ (erg s ⁻¹)	δ_1	δ_2	$\log E_{p,0}$ (keV)	$\log k$	$\log \rho_0$ (GRB Gpc ⁻³ yr ⁻¹)
Amati-like relation $E_p \propto L^{0.43}$								
3 ^a	50.3 ± 0.7		53.5 ± 0.4	1.54 ± 0.18			-6.0 ± 0.2	-0.8 ± 0.2
1	45	50.4 ± 0.5	53.5	0.65 ± 0.22	1.71 ± 0.07		-5.2 ± 0.3	0.0 ± 0.3
2	45	50.5 ± 0.4	53.5	0.62 ± 0.20	1.71 ± 0.09		-5.3 ± 0.2	-0.1 ± 0.2
3	45	51.2 ± 0.6	53.5	0.60 ± 0.22	1.71 ± 0.22		-5.9 ± 0.2	-0.7 ± 0.2
3	46	51.1 ± 0.7	53.5	0.64 ± 0.20	1.70 ± 0.29		-5.9 ± 0.2	-0.7 ± 0.2
3	47	51.2 ± 0.6	53.5	0.69 ± 0.24	1.70 ± 0.30		-5.8 ± 0.2	-0.6 ± 0.2
3	48	51.3 ± 0.5	53.5	0.74 ± 0.27	1.75 ± 0.38		-5.8 ± 0.2	-0.6 ± 0.2
3	49	51.6 ± 1.1	53.5	1.02 ± 0.45	1.98 ± 0.72		-5.7 ± 0.2	-0.5 ± 0.2
3	50	52.0 ± 1.2	53.5	1.47 ± 0.65	2.05 ± 0.86		-5.9 ± 0.1	-0.7 ± 0.1
log-normal peak energy distribution								
3 ^a	50.5 ± 1.3		53.7 ± 0.9	1.52 ± 0.48		2.79 ± 0.08	-6.2 ± 0.2	-1.0 ± 0.2
1	45	51.2 ± 0.4	53.5	0.67 ± 0.23	1.80 ± 0.16	2.80 ± 0.11	-5.5 ± 0.2	-0.3 ± 0.2
2	45	51.5 ± 0.5	53.5	0.71 ± 0.21	2.04 ± 0.57	2.75 ± 0.09	-5.6 ± 0.3	-0.5 ± 0.3
3	45	52.1 ± 0.5	53.5	0.66 ± 0.20	2.37 ± 0.71	2.80 ± 0.08	-6.1 ± 0.2	-0.9 ± 0.2

^a Preferred model in the case of a single power-law LF (Daigne et al. 2006).

bars. There is therefore a discrepancy for the low-luminosity slope which is flatter in their case. We believe however that the use of a more realistic spectral shape together with a constraint on the peak energy distribution leads in our case to a better determined LF at low luminosity.

The two important results from this new set of Monte Carlo simulations are that (1) a broken power-law is compatible with present data but is not preferred compared to a single power-law (equally good fits of the observations); (2) if the LF is indeed a broken power-law, the low-luminosity slope is constrained to be $\delta_1 \simeq 0.6 \pm 0.2$ (Amati-like relation) or $\delta_1 \simeq 0.7 \pm 0.2$ (log-normal peak energy distribution), i.e. compatible with the prediction of the internal shock model derived in Sect.2.

3.3 The rate of underluminous GRBs

A by-product of this study is an estimate of the local GRB rate, which is given in table 1 and is typically, in the SFR₃ scenario, 0.1 – 0.3 GRB Gpc⁻³ yr⁻¹ in the Amati-like case, and 0.08 – 0.2 GRB Gpc⁻³ yr⁻¹ for a log-normal peak energy distribution. This is in good agreement with the results of Guetta & Piran (2007). Despite the fact that our broken power-law LF can in principle extend to very low-luminosity, such a low local rate corresponds to less than 10⁻³ GRB yr⁻¹ within 100 Mpc, which cannot explain the observation of GRB 980425 at z=0.008 or GRB 060618 at z=0.03. As shown in Daigne & Mochkovitch (2007), such underluminous bursts are well explained in the framework of the internal shock model by mildly relativistic / mildly energetic outflows. This would then indicate that the collapsing stars capable to generate such outflows, less extreme than those required to produce standard GRBs, are very numerous and should then produce an additional component in the LF, dominant at very low luminosity. This new branch cannot be the simple continuation of the LF of standard

GRBs derived in this paper. Recently Liang et al. (2007) have studied such a two component LF and found that the local rate corresponding to the low-luminosity component has to be several orders of magnitude above that of standard GRBs but can still represent only a fraction of all type Ib/c supernovae.

4 CONCLUSION

We have demonstrated that in the framework of the internal shock model, a two branch LF is naturally expected, with a predicted low-luminosity branch which is a power-law of slope close to -0.5. This result is robust as long as the central engine responsible for GRBs is capable to produce a broad diversity of outflows, from highly variable to very smooth.

Using a set of Monte Carlo simulations, we have then shown that current observations (log *N* – log *P* diagram, peak energy distribution, fraction of XRRs and XRFs) are compatible with a broken power-law LF but still do not exclude a single power-law distribution. The low-luminosity slope of the broken power-law is strongly constrained to be $\delta_1 \simeq 0.4 - 0.9$, compatible with the prediction of the internal shock model.

These results are encouraging but only preliminary. A better determination of the GRB LF would provide an interesting test of the internal shock model when the low luminosity branch becomes more easily accessible. This will however require the difficult task of detecting many bursts at the threshold of current instruments and measuring their redshift and spectral properties.

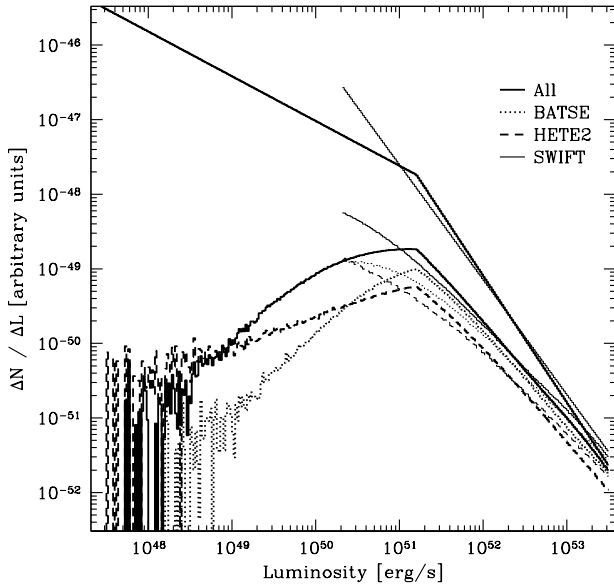


Figure 5. Luminosity function in the scenario SFR_3 + Amati-like relation. The apparent LF, as well as the luminosity distribution of bursts detected by BATSE, HETE2 and SWIFT are plotted in thick line for the best model using a broken power-law with fixed minimum and maximum luminosities $L_{\min} = 10^{45} \text{ erg s}^{-1}$ and $L_{\max} = 10^{53.5} \text{ erg s}^{-1}$. All other parameters can be found in table 1. For comparison the best model for a single power-law LF obtained in Daigne et al. (2006) is plotted in thin line. **Despite the fact that this figure was obtained with a special run simulating 10^9 GRBs with the best model parameters, the curves are very noisy at low luminosity, as these events are very rare.**

ACKNOWLEDGMENTS

HZ is supported by a BAF (Bourse Algéro-Française) No. 40/ENS./FR/2006/2007.

REFERENCES

- Amati L., 2006, MNRAS, 372, 233
 Amati L., Frontera F., Tavani M., in't Zand J. J. M., Antonelli A., Costa E., Feroci M., Guidorzi C., Heise J., Masetti N., Montanari E., Nicastro L., Palazzi E., Pian E., Piro L., Soffitta P., 2002, A&A, 390, 81
 Band D., et al., 1993, ApJ, 413, 281
 Band D. L., Preece R. D., 2005, ApJ, 627, 319
 Barraud C., Daigne F., Mochkovitch R., Atteia J. L., 2005, A&A, 440, 809
 Daigne F., Mochkovitch R., 1998, MNRAS, 296, 275
 Daigne F., Mochkovitch R., 2003, MNRAS, 342, 587
 Daigne F., Mochkovitch R., 2007, A&A, 465, 1
 Daigne F., Rossi E. M., Mochkovitch R., 2006, MNRAS, 372, 1034
 Fenimore E. E., Ramirez-Ruiz E., 2000, astro-ph/0004176
 Firmani C., Avila-Reese V., Ghisellini G., Tutukov A. V., 2004, ApJ, 611, 1033
 Frail D. A., Kulkarni S. R., Sari R., Djorgovski S. G., Bloom J. S., Galama T. J., Reichart D. E., Berger E., Harrison

- F. A., Price P. A., Yost S. A., Diercks A., Goodrich R. W., Chaffee F., 2001, ApJL, 562, L55
 Ghirlanda G., Ghisellini G., Firmani C., Celotti A., Bosnjak Z., 2005, MNRAS, 360, L45
 Guetta D., Piran T., 2007, Journal of Cosmology and Astro-Particle Physics, 7, 3
 Guetta D., Piran T., Waxman E., 2005, ApJ, 619, 412
 Kistler M. D., Yuksel H., Beacom J. F., Stanek K. Z., 2007, astro-ph/0709.0381, 709
 Le T., Dermer C. D., 2007, ApJ, 661, 394
 Liang E., Zhang B., Virgili F., Dai Z. G., 2007, ApJ, 662, 1111
 Nakar E., Piran T., 2005, MNRAS, 360, L73
 Porciani C., Madau P., 2001, ApJ, 548, 522
 Preece R. D., Briggs M. S., Mallozzi R. S., Pendleton G. N., Paciesas W. S., Band D. L., 2000, ApJS, 126, 19
 Rees M. J., Meszaros P., 1994, ApJL, 430, L93
 Sakamoto T., et al., 2005, ApJ, 629, 311
 Soderberg A. M., Kulkarni S. R., Berger E., Fox D. W., Sako M., Frail D. A., Gal-Yam A., Moon D. S., Cenko S. B., Yost S. A., Phillips M. M., Persson S. E., Freedman W. L., Wyatt P., Jayawardhana R., Paulson D., 2004, Nat, 430, 648
 Stern B. E., Atteia J.-L., Hurley K., 2002, ApJ, 578, 304
 Stern B. E., Tikhomirova Y., Kompaneets D., Svensson R., Poutanen J., 2001, ApJ, 563, 80
 Stern B. E., Tikhomirova Y., Stepanov M., Kompaneets D., Berezhnoy A., Svensson R., 2000, ApJL, 540, L21
 Stern B. E., Tikhomirova Y., Svensson R., 2002, ApJ, 573, 75
 Yamazaki R., Yonetoku D., Nakamura T., 2003, ApJL, 594, L79
 Yonetoku D., Murakami T., Nakamura T., Yamazaki R., Inoue A. K., Ioka K., 2004, ApJ, 609, 935